Article

Synthesis and Characterization of BaSO$_4$−CaCO$_3$−Alginate Nanocomposite Materials as Contrast Agents for Fine Vascular Imaging

Mohammad S. Kader, Conner Weyer, Abigail Avila, Samuel Stealey, Scott Sell, Silviya P. Zustiak, Steven Buckner,* Sara McBride-Gagyi,* and Paul A. Jelliss*

Cite This: ACS Mater. Au 2022, 2, 260−268

Read Online

ACCESS | Metrics & More | Article Recommendations | Supporting Information

ABSTRACT: Microcomputed tomography is an important technique for distinguishing the vascular network from tissues with similar X-ray attenuation. Here, we describe a composite of barium sulfate (BaSO$_4$) nanoparticles, calcium carbonate (CaCO$_3$) nanoparticles, and alginate that provides improved performance over microscale BaSO$_4$ particles, which are currently used clinically as X-ray contrast agents. BaSO$_4$ and CaCO$_3$ nanoparticles were synthesized using a polyol method with tetraethylene glycol as solvent and capping agent. The nanoparticles show good colloidal stability in aqueous solutions. A deliverable nanocomposite gel contrast agent was produced by encapsulation of the BaSO$_4$ and CaCO$_3$ nanoparticles in an alginate gel matrix. The gelation time was controlled by addition of D-(+)-gluconic acid δ-lactone, which controls the rate of dissolution of the CaCO$_3$ nanoparticles that produce Ca^{2+} which cross-links the gel. Rapid cross-linking of the gel by Ba^{2+} was minimized by producing BaSO$_4$ nanoparticles with an excess of surface sulfate. The resulting BaSO$_4$−CaCO$_3$ nanoparticle alginate gel mechanical properties were characterized, including the gel storage modulus, peak stress and elastic modulus, and radiodensity. The resulting nanocomposite has good viscosity control and good final gel stiffness. The nanocomposite has gelation times between 30 and 35 min, adequate for full body perfusion. This is the first nanoscale composite of a radiopaque metal salt to be developed in combination with an alginate hydrogel and designed for medical perfusion and vascular imaging applications.
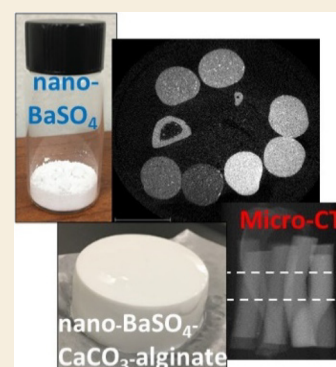
KEYWORDS: barium sulfate nanoparticles, alginate gel, micro-CT

INTRODUCTION

Accurately quantifying vascular networks in biological tissues is of great interest for many biological and biomedical researchers. Historically, this has been achieved with two-dimensional modalities like histology, which are not ideal for small features like blood vessels, where sectioning bias can greatly affect the resultant data.[1] Using a three-dimensional modality allows more accurate measurements and assessment of the entire network in a volume of interest. One technology for 3D measurements is microcomputed tomography (micro-CT), which is an X-ray-based imaging technique. When CT was first introduced in 1970, it marked a significant shift in clinical technology, allowing for nondestructive visualization and the ability to produce three-dimensional images with higher spatial resolution than 5 μm in both in vivo and ex vivo settings.[2] Micro-CT allows for visualization and quantification of microscale vessels within intact tissue specimens of different organs.[3] This strategy has been used to study the vasculature of the kidney, heart, and liver of rodents.[4] Imaging soft tissues like vessels requires the use of a contrast agent, the composition and performance of which are critical for this imaging modality.[5] In addition, because of the narrower diameter of the vascular networks, it is challenging to inject contrast agents at the capillary levels of different organ systems.[6] Postmortem vascular imaging is critical for forensic investigations that do not involve the destruction or disruption of the vasculature to be able to image intact blood vessels with the same premortem structural integrity.[7] Commercially available vascular contrast agents, which are typically based on iodine, erbium, barium, or lead, have been used to study heart, kidney, tumor, nerve, and bone. The commercially available contrast agents have the major disadvantage of being difficult to inject into rodents' bodies due to their small blood vessels which makes perfusion difficult. Moreover, many commercial vascular imaging materials are not adequately radiopaque.[6] Microfil (Flow Tech, Carver, MA) is a lead-based silicon contrast agent that is often used.[8] This is not an issue when imaging vasculature in
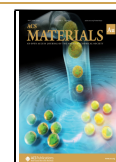
otherwise soft tissues like skin, kidneys, or lungs, but is a major challenge if probing vasculature near dense tissue, such as the bone. Unless the contrast agent is significantly more radiopaque than the bone, it is impossible to segment the two organ systems from a single volume in a single scan. The region must be scanned, decalcified to remove the radiopaque aspects of the bone, and rescanned. The second scan, which contains only the contrast agent-filled vessels, is aligned with and subtracted from the first scan to separate the two tissue types. Having a highly radiopaque vascular contrast agent would not only improve vascular imaging in soft tissues, but it would also greatly streamline vascular imaging in or near the bone.

Nanocomposites can provide improved radiographic contrast for multipurpose imaging due to the delivery of a higher concentration of absorber per particle. Nanocomposites are multicomponent solids in which at least one of the structure's components has a dimension less than or equal to 100 nanometers (nm).[9,10] They have a variety of novel and often controllable characteristics including size, shape, surface functionalization, and morphology, which allow them to be exploited in a wide array of biomedical imaging techniques.[11−13] BaSO$_4$ nanoparticles (BNPs) can provide improvement over microscale BaSO$_4$ particles, currently used clinically as X-ray contrast agents, and should further enable passive or targeted delivery of BaSO$_4$ contrast agents.[14] BNPs have good radio-opacity as well as colloidal stability in aqueous media. Nanoparticles can be encapsulated by a polymer in order to provide stabilization against Ostwald ripening and agglomeration in aqueous media.[15] Previous attempts to synthesize nanoparticles involved direct precipitation by controlling crystal growth and restricting agglomeration using anionic polyelectrolytes,[16] organic polymers,[17] and other additives.[18] Additives and organic polymers prevent agglomeration by acting as a physical barrier at the interface of the nanoparticles with the solution.

One of the most difficult challenges in perfusion is developing a suitable carrier for nanoparticle injection. Initially, the solution must have low viscosity to traverse and fully fill the vascular network from large vessels to capillaries. Then, once the system has been filled, the solution must solidify, while maintaining vessel morphology and preventing premature leakage out of the vascular system either as diffusion into the surrounding tissues or from compromised vessels. It is not unusual for micro-CT scanning to take between 30 and 120 min, and it may not occur hours to days after animal euthanasia. Gelation can produce structures with long-term stability, and timing is another very important factor in gelation for uniform vascular infilling.[14,19] This would allow micro-CT imaging of the vascular structures for extended times and after specimen storage. Premature gelling may result in pressure build up inside the vascular system and subsequent bursting. Alginate, a negatively charged polysaccharide, is a suitable material for applications where gel formation is important and tractable. As a sodium salt, it is soluble in aqueous solution, but formation of a hydrogel occurs upon dissolution with salts of divalent metal cations.[20] Further, alginate gelation is not exothermic, and the entire process can occur at room temperature. Many other gels used as contrast agent carriers require heating to liquefy, which can thermally damage tissues and surrounding vessels, making them inadequate for subsequent histology. As a biocompatible, naturally occurring polysaccharide present in brown algae, alginate has been a valuable biomaterial for cellular transportation without

toxicity.[21] Modification of the alginate gel structures is critical for improving the mechanical and physical properties of the gels and at the same time maintaining sufficient gelation time to allow for perfusion.[22]

We have developed synthetic methods for BaSO$_4$ and CaCO$_3$ nanoparticle (CNP)-containing polymer composites that may find use in vascular imaging techniques with enhanced radiopacity. We propose to develop an effective contrast agent consisting of BNPs, which are uniformly dispersed in an alginate medium that forms a solid composite structure by cross-linking with divalent cations. These nanocomposites demonstrate excellent radiopacity relative to the bone and, moreover, are composed of cheaper materials than current commercial radio contrast agents.

■ EXPERIMENTAL SECTION

Materials

Sodium sulfate (Na$_2$SO$_4$; anhydrate, purity ≥99.0%), sodium carbonate (Na$_2$CO$_3$), barium nitrate [Ba(NO$_3$)$_2$; dihydrate, purity ≥99.0%], alginic acid sodium salt [low viscosity, 4−12 cP, 1% in H$_2$O (25 °C)], poly(ethylene glycol) (MW 10,000 g/mol by GPC), poly(sodium 4-styrenesulfonate) (PSS, MW 70,000 g/mol by GPC), poly(acrylic acid) sodium salt (MW 5100 g/mol by GPC), and D-(+)-gluconic acid δ-lactone (GDL; C$_6$H$_{10}$O$_6$) were purchased from Sigma-Aldrich (St Louis, MO, USA). Calcium chloride (CaCl$_2$; 96% purity, Acros Organics, USA), tetraethylene glycol (TEG; 99%, Alfa Aesar, Thermo Fisher scientific, USA), and polyvinyl alcohol (PVA, MW 30,000 g/mol, Merck KGaA, Germany) were used as supplied. Stock aqueous solutions of 2.0% w/v alginate, used in most experiments, were made by using alginic acid sodium salt powder with deionized (DI) water. After complete dissolution, the aqueous alginate was stored at 4 °C and was used within 1 week of mixing.

Synthesis of BNPs and CNPs

The synthetic protocols for BNPs and CNPs were based on arrested precipitation of BaSO$_4$ and CaCO$_3$. Initially, several different capping agents were investigated: ethylene glycol (EG), polyethylene glycol (PEG), TEG, PVA, PSS, and polyacrylic acid sodium salt (PAA) in order to find the best capping agent capable of producing the smallest size BaSO$_4$ and CaCO$_3$ particles. Ultimately, TEG proved to be the best of these, and so, the synthetic protocols for both BNPs and CNPs reported below incorporate TEG. It should be noted that similar quantities of the other capping agents (PEG, PVA, PSS, and PAA) were used (% of reaction mixture reported in Table 1), with the exception of EG in both BNP and CNP syntheses and TEG in CNP synthesis, at 80 and 94%, respectively. High-intensity sonication using a sonic dismembrator (Model 550, Fisher Scientific) was applied to prevent aggregation during the nanoparticle formation.

Table 1. Different Capping Method Comparisons of BNP and CNP Sizes as Measured by DLS

capping agents	particles size (nm) range (BNPs)	particles size (nm) range (CNPs)
ethylene glycol (EG), 80% (v/v)	1500 ± 30	2500 ± 15
poly (sodium 4-styrenesulfonate) (PSS), 55% (w/v)	2200 ± 50	2000 ± 25
polyacrylic acid sodium salt (PAA), 55% (w/v)	2000 ± 25	3000 ± 30
polyvinyl alcohol (PVA), 45% (w/v)	1700 ± 15	2000 ± 15
polyethelene glycol (PEG), 25% (w/v)	800 ± 12	600 ± 15
tetraetheylene glycol (TEG)[a]	50 ± 5	70 ± 5

[a]TEG was 44% (v/v) for BNPs and 94% (v/v) for CNPs.

BaSO₄ Nanoparticles

In 27 mL of DI water, 10 g of Na_2SO_4 was dissolved to make 2.61 M Na_2SO_4. Separately, 16 g of $Ba(NO_3)_2$ was dissolved in 100 mL of DI water to make 0.61 M $Ba(NO_3)_2$. The $Ba(NO_3)_2$ solution was combined with 100 mL of TEG using a glass rod to promote full dissolution of the TEG. To this mixture was added the Na_2SO_4 solution dropwise with a Pasteur pipette over the course of 10−15 min, while being subjected to high-intensity sonication using the sonic dismembrator. The final TEG concentration after combination was 44% (v/v). The sonic dismembrator was tuned so that it was highly pitched, and the solution was visibly mixed (this was readjusted throughout the addition). Drops of Na_2SO_4 were added closest to the sonic dismembrator probe at a rate of 2 drops per second. After the contents of the pipette were fully dispensed, the beaker was moved so that the probe reached the edges in a circular twisting motion and was then returned to the middle of the beaker. Once the addition was complete, a watch glass was placed on top of the beaker holding the suspended BNPs for 5−6 h. Finally, the BNP solution was centrifuged (3500 rpm, 15 min), and the solid was washed and dried in an oven at 100−150 °C for 10−12 h to yield 10 g of dry white powder.

CaCO₃ Nanoparticles

Into a glass vial was weighed 0.50 g of Na_2CO_3, which was dissolved in 2.0 mL of DI water by shaking to obtain a 2.4 M Na_2CO_3 solution. Separately, 0.50 g of $CaCl_2$, weighed into a glass vial, was dissolved in 1.0 mL of DI water by shaking to obtain a 4.5 M $CaCl_2$ solution. The $CaCl_2$ solution was then combined with 50 mL of TEG using a glass rod to promote complete mixing with the TEG. To this mixture was added the Na_2CO_3 solution dropwise with a Pasteur pipette over the course of 10−15 min, while being subjected to the same manner of high-intensity sonication using the sonic dismembrator as described for the BNP synthesis mentioned above. The final TEG concentration after combination was 94% (v/v). Once the addition was complete, a watch glass was placed on top of the beaker holding the suspended CNPs for 5−6 h. Finally, the CNP solution was centrifuged (3500 rpm, 15 min), and the solid was washed and dried in an oven at 100−150 °C for 10−12 h to yield 0.50 g of dry white powder.

Preparation of Alginate Hydrogel

The following describes the typical production of a gel cylinder produced for gelation time and viscosity analysis. First, 0.20 g of alginic acid sodium salt was added to 5 mL of DI water. Approximately 1.0, 1.5, 2.0, 2.5, 3.0, 3.5, and 4.0 g of the BNP powder was dispersed in 5 mL of DI water to prepare various BNP concentrations of 0.10, 0.15, 0.20, 0.25, 0.30, 0.35, and 0.40 g/mL. Then, 0.20 g of CNPs and 1.0 g of Na_2SO_4 were added to the BNP solution. The BNP solution was then sonicated for 5 min to disperse the NP powders in the solution. Next, the alginic acid sodium salt solutions and BNP suspension were combined. Finally, 0.052 g of GDL was added to the combined mixture and dissolved to initiate the cross-linking. Control gels were similarly prepared for storage modulus and compressive stiffness analysis by inclusion of the same quantities of CNPs and GDL, but with omission of BNPs and/or Na_2SO_4.

Particle Diameter and Dispersibility

Dynamic light scattering (DLS) measurements were recorded using a Zetasizer Ultra (Malvern Panalytical Ltd., Worcestershire, UK), fitted with a 10 mW 632.8 nm helium-neon laser, using noninvasive backscatter with a scattering angle of 173° and the temperature at 25 °C. The particle sizes reported in Table 1 were the average of three measurements. Representative DLS size plots are shown in Figures S1 and S2. Powder X-ray diffraction (PXRD) measurements were carried out with a Rigaku Miniflex 600 X-ray diffractor with Cu Kα radiation (40 kV, 15 mA). Crystalline phases were identified by comparison with the ICDD Crystallographic Database. BNPs were identified as barite (β-$BaSO_4$), ICDD # 01-076-0214 (FoM 0.939), and CNPs were identified as calcite ($CaCO_3$), ICDD # 01-083-4602 (FoM 0.410). The Scherrer equation, $D = K\lambda/\beta\cos\theta$, was used to calculate the crystallite size of nanoparticles with a size distribution, where D is the particle diameter, λ is the wavelength of the X-rays, θ is the

diffraction angle, β is the full-width-at-half-maximum, and K is a constant.[23] The transmission electron microscopy (TEM) samples were prepared by suspending the dried nanoparticles in distilled water and then casting on Formvar TEM grids (Ted Pella). Electron microscopy images were obtained with a JOEL 1200EX TEM instrument operated at 60 kV and a JOEL 1400 Plus (XR 80 Camera) TEM operated at HV = 120 kV.

Gelation Time and Viscosity Measurement

The gelation of alginate hydrogel was studied using the inverted test tube method.[24] The gelation time was determined when the alginate did not flow at the point of inversion during gelation, which was executed every 30 s at room temperature and measured using a stopwatch.[19] Different GDL, alginate, and CNP compositions were tested to obtain the optimal gelation time, while retaining a fixed composition of BNPs and Na_2SO_4 (Table S1). To determine the relative storage modulus and working times of the hydrogel composites, rheometric measurements were taken on an AR 2000ex rheometer (TA Instruments, New Castle, DE). Time sweeps were performed using a flat, parallel plate geometry and a constant 2% strain, angular frequency of 1 Hz, and temperature of 37 °C. The storage moduli in Figure 6A and gelation times shown in Table S1 were the average of three measurements.

Hydrogel Compressive Properties

To determine if solidified gels could withstand postmortem tissue harvesting and other handling, compressive testing was performed. Cylindrical gel samples (21 cm diameter and 10 cm height) were prepared for gelatin, CNPs-alginate, and BNPs−CNPs−alginate formulations and compared with commercially available Microfil samples (MV-122, Flow Tech, Inc., Carver, MA). Specimen thickness was estimated using a Mitutoyo IP54 digital micrometer (Mitutoyo American Corp., Aurora, IL). Then, the gels samples were compressed at an extension rate of 10.0 mm/mm to 50% strain (MTS Criterion, Eden Prairie, MN, 100 N load cell). Peak load was recorded in grams-force using Test Suite Elite software. The peak stress and elastic moduli reported in Table 2 were the average of three measurements.

Table 2. Stress Testing of Gelatin, Microfil, BNP Calcium Carbonate Alginate, and Calcium Carbonate Alginate Gel Cylinders[a]

sample	peak stress, kPa	elastic modulus, kPa
BNP−CNP−alginate gel[b]	25 ± 1	112 ± 5
CNP-alginate gel[c]	16 ± 1	75 ± 2
12% gelatin	91 ± 5	604 ± 5
Microfil	12 ± 1	60 ± 1

[a]All cylinders of diameter 21 cm and height 10 cm. [b]BNP was 25% (w/v) and CNP was 2% (w/v) for BNP−CNP−alginate gel. [c]CNP was 2% (w/v) for CNP-alginate gel.

Radiodensity

Gels with BNP concentrations 0.10, 0.15, 0.20, 0.25, 0.30, 0.35, or 0.40 g/mL were prepared and cast in 4.30 mm diameter vinyl tubes. The tubes with containing gels were embedded into agarose with a formalin-fixed rat tibia for reference. The group of samples were scanned in a single scan with micro-CT (Micro-CT 35, ScanCo Medical, Brüttisellen, Switzerland; X-ray tube potential 70 kVp, integration time 300 ms, X-ray intensity 145 A, isotropic voxel size 10 μm, frame averaging 1, projections 1000, and high-resolution scan). Micro-CT image intensity was converted to radiodensity measured in Hounsfield units (HU) using the formula HU = 1000 × (image intensity − image intensity of water)/(image intensity of water).[25] The radiodensities reported in Figure 7 and Table S2 were the average of three measurements.

RESULTS AND DISCUSSION

Both BNPs and CNPs were separately synthesized and characterized. Initially all capped NPs were analyzed with DLS, which provides information on hydrodynamic diameter of particles, dispersibility, and colloidal stability (i.e., zeta potential). The higher the zeta potential, the greater the repulsion and, as a result, the greater the colloidal dispersion of the particles. Then, particles made with the most promising capping agent, TEG, were then analyzed with PXRD and TEM to confirm the DLS measurements. Additionally, PXRD provides information on crystalline size, while TEM visually conveys information about particle size, irregularities, homogeneity, and shape. The BNPs and CNPs were then combined with aqueous Na-alginate polymer in the presence of GDL, resulting in the formation of a solid gel. Viscoelastic storage modulus was probed as a function of time during the gelation process, and an optimal gelation time was determined. The resulting gels were then tested for mechanical stiffness, and their radiodensity was analyzed by micro-CT measurements to identify an optimal composition for future in vivo testing.

BNP and CNP Syntheses and Characterization

Variation of Capping Agents. Commercially available $Ba(NO_3)_2$ and Na_2SO_4 were combined to produce a precipitate of BNPs. In parallel, $CaCl_2$ and Na_2CO_3 solutions were similarly combined to afford a precipitate of CNPs. Uncontrolled precipitation can result in the formation of large microscale particles. To control and limit the particle growth, capping agents were used to arrest the precipitation reactions and limit particles to the nanodimensional range. These ligands also increased the viscosity of the reaction medium which helps slow the nanoparticle crystal growth. Additionally, high-intensity sonication was applied to prevent particle aggregation during the synthesis.

The different capping agents employed greatly affect final particle size according to initial analysis with DLS (Table 1 and Figures S1 and S2). DLS measurements are expected to capture particle aggregate sizes for nanocomposite material suspended in water, rather than individual crystallite sizes. EG, PSS, PAA, and PVA produced the largest particles in the micron range. PEG capping reduced the particle size to under half a micrometer but was still well over 100 nm. TEG, however, outperformed the other methods, creating particles in the tens of nanometer range for both BNPs and CNPs. Because the goal is to have very small particles that can easily navigate the capillary system without occlusion, TEG was deemed the optimal capping method to create nanoparticles for micro-CT imaging. Thus, these particles were the only ones used for further testing.

The polyol capping method is a well-established and reliable method for controlling the growth of nascent nanoparticles of both elements and compounds.[26,27] In our system, the capping agent binds to surface cations and passivates the surface, thus stabilizing the smaller nanoparticles. The capping agent, depending on molecular size, can also increase the solution viscosity, which also helps to control (slow) the rate of the precipitation reaction. TEG seems to provide an optimal balance between nanoparticle surface coverage and solution viscosity. The polymers, such as PEG, provide high viscosity but because of their size, do not envelope the nanoparticles efficiently. At the other end of the scale, EG can bind efficiently and tightly over the entire nanoparticle surface, but due to its smaller molecular weight, provides lower viscosity in solution.

Particle Size Determination by PXRD, TEM, and DLS

PXRD analysis confirmed the presence of crystalline $BaSO_4$ and $CaCO_3$ phases in TEG-capped BNPs (Figure 1A) and
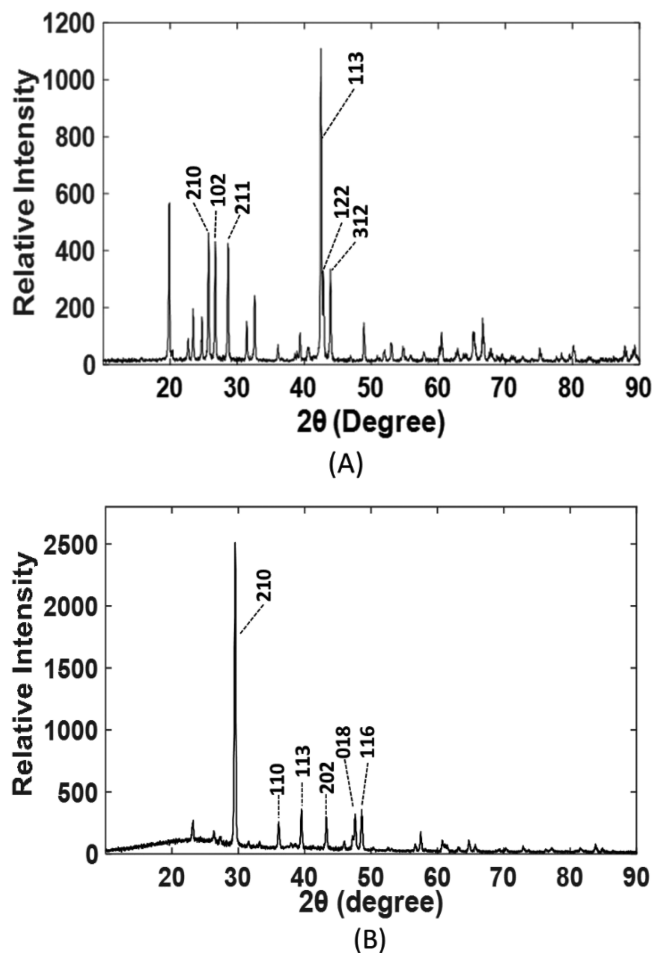
Figure 1. PXRD patterns of (A) BNPs (barite ICDD # 01-076-0214) and (B) CNPs (calcite ICDD # 01-083-4602). For each pattern, the Miller indices of the six most prominent peaks are labeled.

CNPs (Figure 1B), respectively, through identification using the ICDD database. According to Scherrer peak-width-at-half-height analysis, the average TEG-capped BNP diffracting crystallite size was found to be around 35 ± 5 nm and the corresponding TEG-capped CNP crystallite size was found to be 45 ± 6 nm.

The sizes, shape, and morphologies of the BNPs and CNPs were visualized using TEM and the particle diameters of 100 particles were determined from their respective TEM images (Figure 2). The BNP particles were mostly spherical in shape, with some agglomeration observed being most likely due to the TEM grid preparation method (Figure 2A). The particle size distribution is shown in Figure 2B, and the average particle size was determined to be 50 ± 15 nm. This is in agreement with DLS measurements (50 nm), suggesting that individual TEG-capped BNPs do in fact disperse completely in aqueous media. The discrepancy with PXRD crystallite diameters (35 nm) may be attributed to a combination of the nature of the core–shell nanoparticles, with an amorphous capping layer of TEG and barite, as well as a small degree polycrystallinity within the nanoparticles.
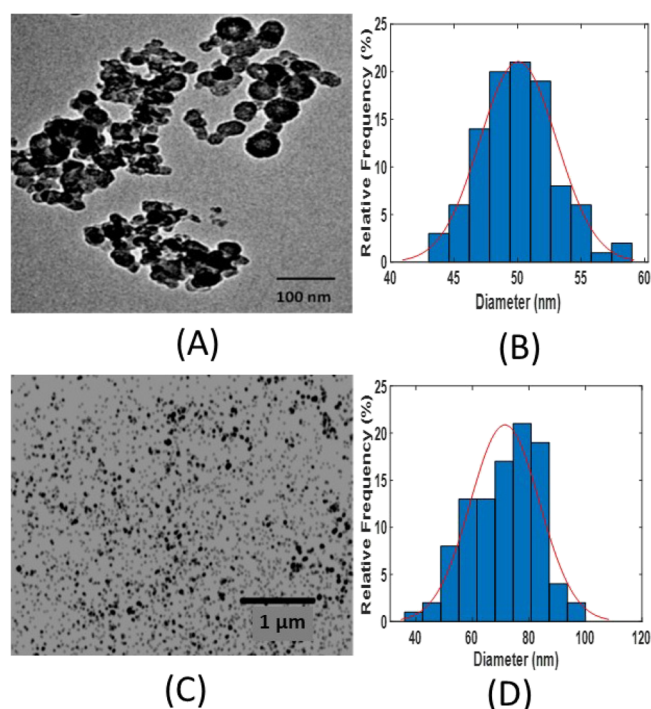
Figure 2. (A) TEM of BNPs capped with TEG, (B) size distribution histogram of BNPs, (C) TEM images of CNPs, and (D) size distribution histogram of CNPs.

Similar TEM analysis of the CNPs showed that the particles were quasi-spherical in shape with little agglomeration (Figure 2C, Figure S3). The particle size distribution is shown in Figure 2D and suggested average CNP diameters of 72 ± 12 nm (Figure 3D). This is again in good agreement with DLS size analysis (70 nm), suggesting that the TEG-capped CNPs also disperse individually in aqueous media. Again, the distinction between PXRD (45 nm)- and TEM/DLS-
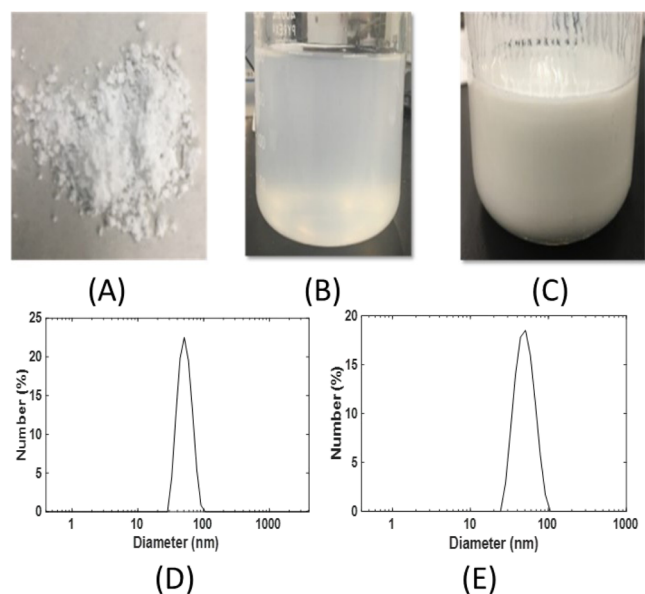
Figure 3. (A) Dry TEG-capped BNP powder, (B) well-dispersed homogenous BNPs in pure liquid TEG, (C) concentrated mixture of homogenous BNPs in pure liquid TEG, (D) DLS size plot of BNPs in liquid TEG, and (E) DLS size plot of CNPs in liquid TEG.

determined particle diameters may be attributed to the amorphous TEG capping layer, estimated to therefore be ca. 12−15 nm.

More detailed DLS analysis permits judgment regarding the colloidal dispersibility and homogeneity of both BNPs and CNPs, something that is important for potential capillary-micro-CT applications. Nanoparticles that aggregate quickly and easily fall out of suspension will resist uniform transportation through capillaries and be more likely to rupture blood vessels during perfusion. Qualitatively, both BNPs and CNPs were found to be very well dispersed in liquid TEG and remained so for more than a week at both low and high solvent loading (Figure 3A−C). DLS sizing analysis revealed that both BNP and CNP colloidal dispersions were homogenous with monomodal size distributions (Figure 3D,E) and with the abovementioned nanoparticle dimensions of 50 ± 5 and 70 ± 5 nm, respectively (Table 1). Both BNPs and CNPs had measured zeta potentials of −41 and −25 mV, respectively (Figure S4). This can be attributed to an exterior nanoparticle surface coating by excess SO_4^{2-} and CO_3^{2-} ions in the BNPs and CNPs, respectively.

Production and Mechanical Properties of BNP−CNP−Alginate Nanocomposite Gels

As a prelude to preparing nanocomposite gel precursor suspensions for capillary perfusion experiments, we developed a synthetic protocol to cast nanocomposite gel cylinders for the purpose of probing the gelling suspension for viscosity and gelling time as well as to examine the mechanical properties of the final cast gel. Alginate was selected as the base gel component because of its tunable mechanical and gelling properties as well as low exothermicity gelling reaction. The precursor liquid nanocomposites were prepared by mixing BNPs, CNPs, GDL, and Na_2SO_4 with a solution of 2% alginic acid sodium salt (2% w/v). GDL is converted to gluconic acid in the presence of water (Figure 4), which slowly lowers the
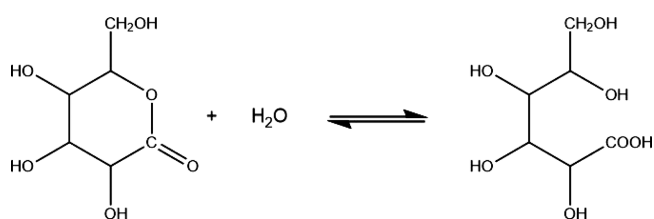
Figure 4. Transformation of D-(+)-gluconic acid δ-lactone (GDL) to gluconic acid in the presence of water.

pH of the solution (Figure S5). In the pH range 6.0−6.5, $CaCO_3$ in the CNPs dissociates, releasing Ca^{2+} and CO_3^{2-} ions into the solution. The free Ca^{2+} cations cross-link with the alginate polymer, slowly transforming the liquid nanocomposite into a solid gel. The cross-linking effects a more rigid long-range order according to the so-called 'egg-box' model of divalent cation binding with the alginate hexose rings (Figure 5).[28] It should be noted that even larger Group 2A metal dications such as Ba^{2+} are also capable of similarly cross-linking the alginate. However, in order not to over-accelerate the cross-linking process, which would be detrimental for complete vasculature perfusion prior to gelation, we added Na_2SO_4 solute to suppress the free Ba^{2+} ion concentration in solution by simply exploiting the common ion effect to reduce the solubility of $BaSO_4$. The resulting gel cylinders are shown in Figure 5B.
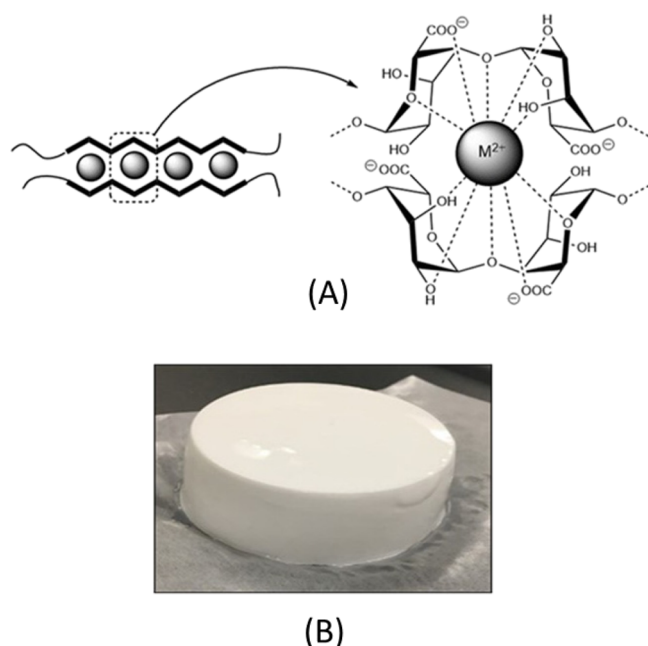
Figure 5. (A) Egg-box model of metal dication-alginate binding and (B) alginate hydrogel disc comprising the BNP/CNP nanocomposite.

In order to determine an optimal gelation time, compositions of CNPs, GDL, and alginate (the primary components that determine the gelation rate) were varied, and the gel formation was studied using the inverted test tube method. Our analysis is guided by the need to form a structurally stable, but flexible, solid gel that can be adequately injected and perfused into the vasculature as a liquid precursor prior to the said solidification. It is generally considered that for perfusion into the arterial system of a rat/mouse, a gelation time of ca. 30–60 min would be ideal. Less than this and the gel would solidify too quickly before it could fully infiltrate smaller capillaries and would be more likely to cause vessels to burst. Too long a gelation time, or incomplete gelation even, and leakage of the nanocomposite components would likely occur before or during micro-CT analysis. The gelation times for an array of CNP/GDL/alginate compositions are presented in Table S1.

Rheological assessment of storage modulus versus time was used to gauge viscosity during the gelation process. Results are presented in Figure 6A. Background measurements of pure DI water and 2% (w/v) alginic acid sodium salt were carried out. As expected, both storage moduli of pure water and the ungelled alginate solution remained constant and low (<50 Pa). Inclusion of the CNPs and GDL, did lead to an increase of storage modulus to just over ca. 1.4×10^3 Pa after ca. 1 h of mixing, with very little change beyond this time. This verified that the chosen CNP content together with the optimized quantity of GDL determined from the inverted tube gelation experiments achieved the objective of gelation on an appropriate timescale for perfusion. Finally, inclusion of BNPs [25% (w/v)] and Na_2SO_4 [10% (w/v)] along with the CNPs [2% (w/v)] and GDL in the gel preparation protocol resulted in the storage modulus plateauing after ca. 2 h at ca. 2.2×10^4 Pa. This is unsurprising, given the high loading of both CNP and BNP nanoparticles. We note, however, that the storage modulus rises to ca. 10^3 Pa within 30 min gelation time. This is about the same as the
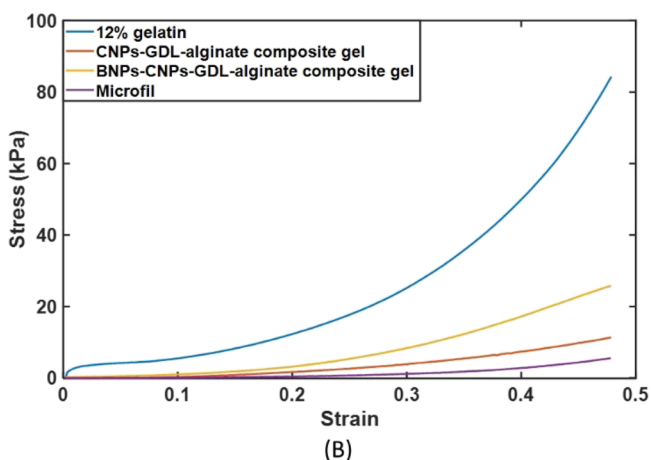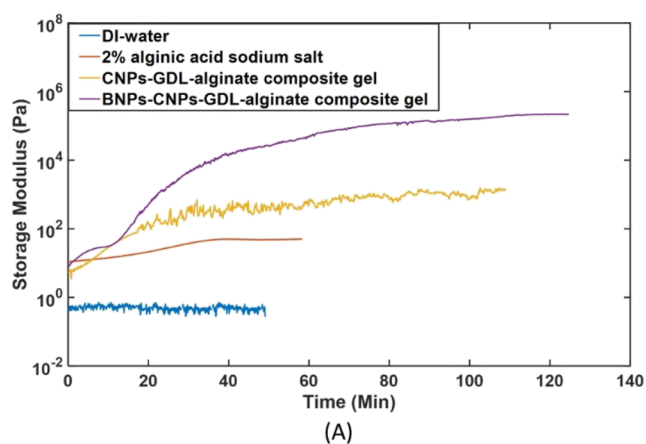
Figure 6. (A) Storage modulus vs time for DI water, 2% alginic acid sodium salt, CNPs−GDL−alginate composite and BNPs−CNPs−GDL−alginate composite gels; (B) stress−strain curve for 12% gelatin, Microfil, CNPs−GDL−alginate composite, and BNPs−CNPs−GDL−alginate composite gels.

maximum measured value for the sample without BNPs present and suggests that this is the time at which gelation to the solid phase has occurred sufficiently such that any perfusion beyond this point would not be recommended. Thus, a working perfusion window of 30−35 min after mixing is optimal for this composition.

Compressive stiffness is another important parameter for the intended micro-CT application because after transforming a liquid composite into a solid gel,[29] the vessel cast must be adequately robust to withstand tissue harvesting and handling without leaching from the vasculature or significantly altering vessel size and shape. Solidified 12% commercial gelatin provides an ideal mechanical stiffness for a solid gel scaffold with entrapped nanoparticles intended for micro-CT imaging, as confirmed in Figure 6B, and with a peak stress value of 91 kPa, as reported in Table 2. However, gelatin has a significant disadvantage, in that it must be forced into solution by heating and remain viscous enough for injection, which is undesirable for micro-CT applications. The high temperature required during injection may cause tissue damage, rendering the sample useless for further experiments like histological analysis. The current industry standard for micro-CT analysis is Microfil, a silicon-based composite material. The mechanical stiffness is the lowest of the four samples studied (Figure 6B) with a peak stress value of just 12 kPa. The CNP-alginate gel

showed greater stiffness, and when BNPs [25% (w/v)] were also incorporated in the nanocomposite along with the CNPs [2% (w/v)], peak stress was recorded at 25 kPa. While not as stiff as the gelatin, it is a marked improvement over the Microfil.

Radiodensity of Nanocomposite Gels

Nanocomposite radiodensity will be critical for distinguishing the vascular networks into which they have been injected, especially in volumes that contain radiodense tissues like the bone. As the concentration of heavily X-ray scattering elements such as barium increases, so should the radiodensity of the nanocomposite. Gels with seven distinct BNP concentrations ranging from 0.10 to 0.40 g/mL were prepared and cast in vinyl tubes. The samples were collectively embedded into agarose along with a formalin-fixed rat tibia for reference and scanned by micro-CT to determine their radiodensity and establish the minimum concentration needed for differentiation from bone (Figure 7A,B). The progressive increase
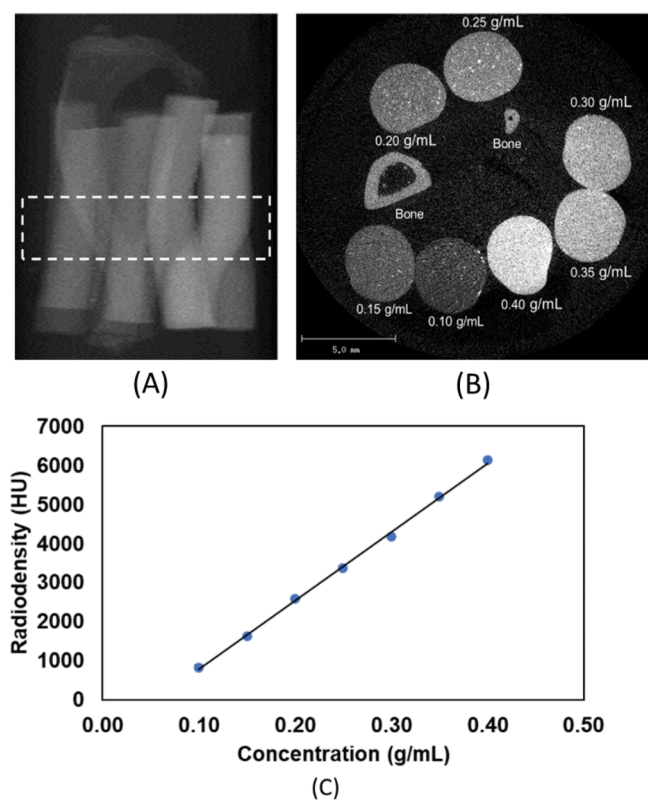
Figure 7. (A) Micro-CT scout view of the BNPs−CNPs−GDL− alginate composite gels. (B) Micro-CT scanning of the BNPs− CNPs−GDL−alginate composite gels at different concentrations (0.10−0.40 g/mL) of BNPs, and (C) calibration curve of BNPs conc. vs radiodensity based on measurements given in Table S2.

in radiodensity is evident, and in comparison with the embedded rat tibia, the highest concentration of BNPs studied (0.40 g/mL) clearly yields a much brighter image. The measured X-ray intensity may be converted to radiodensity HU (Table S2) and plotted versus BNP concentration in the gels, affording a clearly linear relationship (Figure 7C). However, as storage modulus of the injected gelating solution also increases with BNP concentration in the suspension, it is also incumbent upon us to identify the minimal BNP loading needed for adequate imaging.

The images in Figure 7 suggest that the minimum BNP loading should thus be greater than 0.25 g/mL (3378 HU) because the radiodensity for this sample is roughly the same as that as for the rat tibia (3158 HU) and higher than that for Microfil (750 HU) at the same X-ray intensity threshold, which is shown for comparison in Figure S6. Several bright spots are noted in the images and can be attributed to some patchy agglomeration within the gel structure once set. This does not appear to be a function of the age or shelf-life of the nanoparticles, as they are stable and do not degrade (as determined by PXRD analysis of nanoparticles that are several months old).

Figure 8 depicts the radiodensity of the various concentrated nanocomposites at various X-ray intensity threshold levels. The
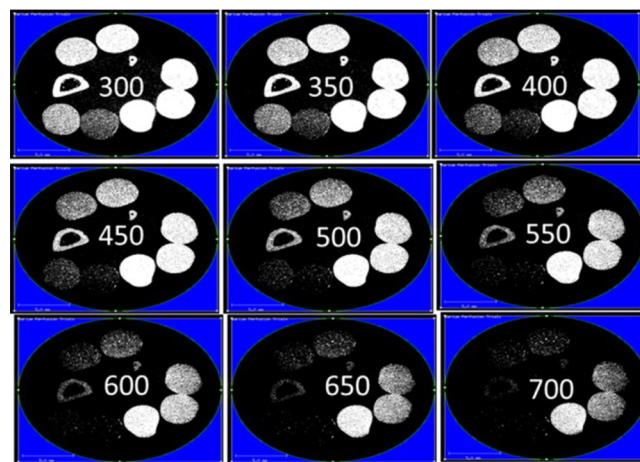
Figure 8. Micro-CT scanning at different X-ray intensity thresholds (300−700 permilles).

images show that at the 700 permilles X-ray threshold, only concentrations greater than 0.25 g/mL were uniformly visible. This confirms that at least 0.30 g/mL BNP concentration in the gel is required to be visible at higher threshold X-ray scanning.

■ CONCLUSIONS

In this research, BNPs and CNPs (<100 nm) were synthesized and incorporated into alginate gels for potential applications in postmortem micro-CT vascular network imaging. CNP composition was optimized to control gelation time to within a 30−35-minute window, which would be adequate for full perfusion of mouse vasculature. The stiffness of the developed nanocomposite gel was shown to be improved over that of commercially available Microfil. Finally, micro-CT analysis determined that the minimal nanocomposite radiodensity for studying the vasculature in the vicinity of bone could be achieved with a BNP concentration of 0.30 g/mL in the injected gelating suspension. Two principal benefits of this new nanocomposite material include the cheap cost of the constituent materials as well as avoiding the need to apply heat to achieve the injection and gelation process.

■ ASSOCIATED CONTENT

Ⓢ Supporting Information

The Supporting Information is available free of charge at https://pubs.acs.org/doi/10.1021/acsmaterialsau.1c00070.

Size distribution plots determined by DLS for both BNPs and CNPs in EG, PSS, PAA, PVA, and PEG; TEM image of CNPs at high magnification; plots of zeta potential measurements of BNPs and CNPs in water; plot of pH change with time of GDL-promoted gel solutions; micro-CT scanning of the BNPs–CNPs–GDL–alginate composite gels at different concentrations (0.10–0.40 g/mL) of BNPs and Microfil; table of gelation times determined by the inverted test tube method; and table of stress testing results for BNPs–CNPs–alginate and CNPs–alginate gel formulations (PDF)

AUTHOR INFORMATION

Corresponding Authors

Steven Buckner − *Department of Chemistry, Saint Louis University, St. Louis, Missouri 63103, United States;* orcid.org/0000-0003-3630-0753; Email: steven.buckner@slu.edu

Sara McBride-Gagyi − *Department of Orthopaedic Surgery, Saint Louis University School of Medicine, St. Louis, Missouri 63110, United States*; Email: sara.mcbridegagyi@health.slu.edu

Paul A. Jelliss − *Department of Chemistry, Saint Louis University, St. Louis, Missouri 63103, United States;* orcid.org/0000-0002-7578-0350; Email: paul.jelliss@slu.edu

Authors

Mohammad S. Kader − *Department of Chemistry, Saint Louis University, St. Louis, Missouri 63103, United States*

Conner Weyer − *Department of Chemistry, Saint Louis University, St. Louis, Missouri 63103, United States*

Abigail Avila − *Department of Biomedical Engineering, Parks College of Engineering, Aviation and Technology, Saint Louis University, St. Louis, Missouri 63103, United States*

Samuel Stealey − *Department of Biomedical Engineering, Parks College of Engineering, Aviation and Technology, Saint Louis University, St. Louis, Missouri 63103, United States*

Scott Sell − *Department of Biomedical Engineering, Parks College of Engineering, Aviation and Technology, Saint Louis University, St. Louis, Missouri 63103, United States*

Silviya P. Zustiak − *Department of Biomedical Engineering, Parks College of Engineering, Aviation and Technology, Saint Louis University, St. Louis, Missouri 63103, United States;* orcid.org/0000-0002-7648-8351

Complete contact information is available at:
https://pubs.acs.org/10.1021/acsmaterialsau.1c00070

Author Contributions

The manuscript was written through contributions of all authors. All authors have given approval to the final version of the manuscript.

Notes

The authors declare no competing financial interest.

ABBREVIATIONS

BNPs barium sulfate nanoparticles
CNPs calcium carbonate nanoparticles
GDL D-(+)-gluconic acid δ-lactone
EG ethylene glycol
PEG polyethylene glycol
TEG tetraethylene glycol
PVA polyvinyl alcohol
PSS poly(sodium 4-styrenesulfonate)
PAA polyacrylic acid sodium salt
DLS dynamic light scattering
PXRD powder X-ray diffraction
FoM figure of merit
TEM transmission electron microscopy

REFERENCES

(1) Brown, D. L. Bias in image analysis and its solution: unbiased stereology. *J. Toxicol. Pathol.* **2017**, *30*, 183−191.
(2) Burghardt, A. J.; Link, T. M.; Majumdar, S. High-resolution computed tomography for clinical imaging of bone microarchitecture. *Clin. Orthop. Relat. Res.* **2011**, *469*, 2179−2193.
(3) Tse, J. J.; Dunmore-Buyze, P. J.; Drangova, M.; Holdsworth, D. W. Erbium-Based Perfusion Contrast Agent for Small-Animal Microvessel Imaging. *Contrast Media Mol. Imaging* **2017**, *2017*, No. 7368384.
(4) Cruje, C.; Dunmore-Buyze, P. J.; Grolman, E.; Holdsworth, D. W.; Gillies, E. R.; Drangova, M. PEG-modified gadolinium nanoparticles as contrast agents for in vivo micro-CT. *Sci. Rep.* **2021**, *11*, 16603.
(5) Paques, J. P.; van der Linden, E.; van Rijn, C. J.; Sagis, L. M. Preparation methods of alginate nanoparticles. *Adv. Colloid Interface Sci.* **2014**, *209*, 163−171.
(6) Zagorchev, L.; Oses, P.; Zhuang, Z. W.; Moodie, K.; Mulligan-Kehoe, M. J.; Simons, M.; Couffinhal, T. Micro computed tomography for vascular exploration. *J. Angiog. Res.* **2010**, *2*, 7−7.
(7) Ross, S. G.; Bolliger, S. A.; Ampanozi, G.; Oesterhelweg, L.; Thali, M. J.; Flach, P. M. Postmortem CT Angiography: Capabilities and Limitations in Traumatic and Natural Causes of Death. *RadioGraphics* **2014**, *34*, 830−846.
(8) Vasquez, S. X.; Gao, F.; Su, F.; Grijalva, V.; Pope, J.; Martin, B.; Stinstra, J.; Masner, M.; Shah, N.; Weinstein, D. M.; Farias-Eisner, R.; Reddy, S. T. Optimization of MicroCT Imaging and Blood Vessel Diameter Quantitation of Preclinical Specimen Vasculature with Radiopaque Polymer Injection Medium. *PLoS One* **2011**, *6*, No. e19099.
(9) Malhotra, B. D.; Ali, M. A.; Chapter 5 − Nanocomposite Materials: Biomolecular Devices. In *Nanomaterials for Biosensors*; Malhotra, B. D.; Ali, M. A., Eds.; William Andrew Publishing, 2018; pp 145 −159.
(10) Kader, M. S.; Chusuei, C. C. A Cobalt (II) Oxide Carbon Nanotube Composite to Assay Dopamine. *Chemosensors* **2020**, *8*, 22.
(11) Wang, E. C.; Wang, A. Z. Nanoparticles and their applications in cell and molecular biology. *Integr. Biol.* **2013**, *6*, 9−26.
(12) Camargo, P. H. C.; Satyanarayana, K. G.; Wypych, F. Nanocomposites: synthesis, structure, properties and new application opportunities. *Mater. Res.* **2009**, *12*, 1−39.
(13) Paul, D. R.; Robeson, L. M. Polymer nanotechnology: Nanocomposites. *Polymer* **2008**, *49*, 3187−3204.
(14) Gillani, R.; Ercan, B.; Qiao, A.; Webster, T. J. Nano-functionalized zirconia and barium sulfate particles as bone cement additives. *Int. J. Nanomed.* **2010**, *5*, 1−11.
(15) Ferrara, T. P.; Clemett, A. R. Radiographic Contrast Agents. *Radiology* **1978**, *126*, 602−602.
(16) Baez, E.; Quazi, N.; Ivanov, I.; Bhattacharya, S. N. Stability study of nanopigment dispersions. *Adv. Powder Technol.* **2009**, *20*, 267−272.
(17) Wang, Y.; Dave, R. N.; Pfeffer, R. Polymer coating/encapsulation of nanoparticles using a supercritical anti-solvent process. *J. Supercrit. Fluids* **2004**, *28*, 85−99.
(18) Yang, Y.; Chen, H.; Zhao, B.; Bao, X. Size control of ZnO nanoparticles via thermal decomposition of zinc acetate coated on organic additives. *J. Cryst. Growth* **2004**, *263*, 447−453.

(19) Growney Kalaf, E. A.; Flores, R.; Bledsoe, J. G.; Sell, S. A. Characterization of slow-gelling alginate hydrogels for intervertebral disc tissue-engineering applications. *Mater. Sci. Eng., C* **2016**, *63*, 198−210.

(20) Loureiro dos Santos, L. A. Natural Polymeric Biomaterials: Processing and Properties☆. In *Reference Module in Materials Science and Materials Engineering*; Elsevier, 2017.

(21) Kim, A. R.; Hwang, J. H.; Kim, H. M.; Kim, H. N.; Song, J. E.; Yang, Y. I.; Yoon, K. H.; Lee, D.; Khang, G. Reduction of inflammatory reaction in the use of purified alginate microcapsules. *J. Biomater. Sci., Polym. Ed.* **2013**, *24*, 1084−1098.

(22) Drury, J. L.; Mooney, D. J. Hydrogels for tissue engineering: scaffold design variables and applications. *Biomaterials* **2003**, *24*, 4337−4351.

(23) Ito, T.; Sun, L.; Bevan, M. A.; Crooks, R. M. Comparison of Nanoparticle Size and Electrophoretic Mobility Measurements Using a Carbon-Nanotube-Based Coulter Counter, Dynamic Light Scattering, Transmission Electron Microscopy, and Phase Analysis Light Scattering. *Langmuir* **2004**, *20*, 6940−6945.

(24) Eldridge, J. E.; Ferry, J. D. Studies of the Cross-linking Process in Gelatin Gels. III. Dependence of Melting Point on Concentration and Molecular Weight. *J. Phys. Chem.* **1954**, *58*, 992−995.

(25) Hainfeld, J. F.; O'Connor, M. J.; Dilmanian, F. A.; Slatkin, D. N.; Adams, D. J.; Smilowitz, H. M. Micro-CT enables micro-localisation and quantification of Her2-targeted gold nanoparticles within tumour regions. *Br. J. Radiol.* **2011**, *84*, 526−533.

(26) Lee, G. H.; Chang, Y.; Kim, T.-J. 3 − Synthesis and surface modification. In *Ultrasmall Lanthanide Oxide Nanoparticles for Biomedical Imaging and Therapy*; Lee, G. H.; Chang, Y.; Kim, T.-J., Eds.; Woodhead Publishing, 2014; pp 29−41.

(27) Bensebaa, F. Chapter 2 − Wet Production Methods. In *Interface Science and Technology*; Bensebaa, F., Ed.; Elsevier, 2013; Vol. 19, pp 85−146.

(28) Lee, K. Y.; Mooney, D. J. Alginate: Properties and biomedical applications. *Prog. Polym. Sci.* **2012**, *37*, 106−126.

(29) Zeng, L.; Song, M.; Gu, J.; Xu, Z.; Xue, B.; Li, Y.; Cao, Y. A Highly Stretchable, Tough, Fast Self-Healing Hydrogel Based on Peptide−Metal Ion Coordination. *Biomimetics* **2019**, *4*, 36.